Energy Storage and Hydrogen Production by Proton Conducting Solid Oxide Electrolysis Cells with A Novel Heterogeneous Design

Libin Lei [a,c], Jihao Zhang [c,d], Rongfeng Guan [b], Jianping Liu [a], Fanglin Chen [c], Zetian Tao [b,c*]

[a] Smart Energy Research Center, School of Materials and Energy, Guangdong University of Technology, Guangzhou 510006, PR China.

[b] Key Laboratory for Advanced Technology in Environmental Protection of Jiangsu Province, Yancheng Institute of Technology, Yancheng 224051, P. R. China. E-mail: newton@mail.ustc.edu.cn.

[c] Department of Mechanical Engineering, University of South Carolina, Columbia, SC 29208, USA.

[d] State Key Laboratory of Power Systems, Department of Thermal Engineering, Tsinghua University, Beijing 100084, P.R. China

Abstract: The proton-conducting solid oxide electrolysis cell is a promising technology for energy storage and hydrogen production. However, because of the aggressive humid condition in the air electrode side, the stability of electrolysis cells is still a concern. In addition, the energy efficiency needs further improvement before its practical application. In this work, considering both stability and energy efficiency, a novel heterogeneous design is proposed for proton-conducting solid oxide electrolysis cells. In this heterogeneous design, the merits of proton-conducting materials can be taken advantage of and the drawbacks of proton-conducting materials can be circumvented synchronously, resulting in better stability and higher efficiency of electrolysis cells. The feasibility and advantages of the heterogeneous design are demonstrated in electrolysis cells with yttrium and zirconium co-doped barium cerate-nickel as the fuel electrode material and yttrium-doped

barium zirconate as the electrolyte material by experiment and modeling. The experimental results demonstrate that compared with the conventional homogeneous design, this novel design can efficiently improve the proton conductivity of the yttrium-doped barium zirconate electrolyte (from 0.88×10^{-3} S cm^{-1} to 2.13×10^{-3} S cm^{-1} at 873 K) and slightly improve the ionic transport number of the electrolyte (from 0.941 to 0.964 at 873 K), resulting in better electrochemical performance. The electrolysis cells with this design also show good stability. Moreover, the simulation results show that the faradaic efficiency and energy efficiency of electrolysis cells are improved by applying this novel design. These impressive results demonstrate that heterogeneous design is a rational design for high-performance and efficient proton-conducting solid oxide electrolysis cell.

Keywords: hydrogen production; proton conductors; solid oxide electrolysis cells; heterogeneous design; energy efficiency

Nomenclature

Nomenclature			
Abbreviation		*English letter*	
H-SOEC	proton-conducting solid oxide electrolysis cell	P	pressure (atm)
BZCY17	$BaZr_{0.1}Ce_{0.7}Y_{0.2}O_3$	R_s	apparent ohmic resistance (Ω cm^2)
BZCY	$BaZr_{0.8-x}Ce_xY_{0.2}O_{3-\delta}$	R_i	ionic resistance (Ω cm^2)
BZY	$BaZr_{0.8}Y_{0.2}O_{3-\delta}$	R_e	electronic resistance (Ω cm^2)
SFM	$Sr_2Fe_{1.5}Mo_{0.5}O_{6-\delta}$	R_T	total apparent resistance (Ω cm^2)

OCV	open circuit voltage	R_p	apparent polarization resistance (Ω cm^2)
FE	faradaic efficiency	$R_{p,r}$	real polarization resistance (Ω cm^2)
LHV	lower heating value	t_i	transport number of ions
Greek symbols		E_N	theoretical potential
σ	conductivity (S cm^{-1})	V_{OCV}	measured opon circuit voltage
μ	chemical potential	R	gas constant 8.314 J/(mol K)
Φ	electrostatic potential	*T*	temperature (K)
η	energy efficiency	F	Faraday constant 96485 C/mol
σ	conductivity (S cm^{-1})	J	current density (A cm^{-2})
Subscripts		t	time (s)
$h^{\cdot}$	electronic hole	N	production amount (molar)
$OH^{\cdot}$	hydroxy proton		
H_2	hydrogen	Superscripts	
ext	external	*o*	condition at open circuit voltage

1. Introduction

The substantial demands for clean and renewable energy resources have attracted worldwide attention due to the rapid growth of the world's population and economy. Renewable energy sources, such as solar, wind, and tidal energy, have been greatly promoted in recent decades to achieve a sustainable global energy supply and combat the environmental issues associated with the ever-increasing consumption of fossil fuels[1]. However, these renewable energy sources are

not suitable for continuous energy supply and energy storage devices are needed to store excess energy. Electrolysis cells, which can efficiently convert electrical energy to chemical energy, are promising for large-scale energy storage[2]. Among different types of electrolysis cells, solid oxide electrolysis cells based on proton-conducting electrolyte (H-SOECs) have drawn considerable attention due to their advantages such as lower material cost, higher electrochemical performance and easier gas separation [3].

Fig.1 shows the working principle of H-SOECs. In the fuel electrode side, only dry hydrogen, as the product, is produced, so the stability requirement of fuel electrode material is simple. In the air electrode side, steam is fed as the reactant. Considering the aggressive humid condition, air electrode and electrolyte materials should maintain chemically stable in steam, which imposes a significant restriction on the choice of materials.

Y-doped $BaZrO_3$ (BZY) and $BaZr_{0.8-x}Ce_xY_{0.2}O_{3-\delta}$ (BZCY), have been applied for the state-of-the-art proton-conducting solid oxide fuel cells (H-SOECs) as the proton-conducting electrolyte materials and electrode materials [4]. However, until now, there are still some paramount problems for the application of BZY and BZCY. For BZY, although it possesses excellent chemical stability in an H_2O/CO_2-containing atmosphere [5], it is notorious for its high resistance of grain boundary [6], which could result in significant loss of voltage and energy efficiency of H-SOECs. As for BZCY, although it shows higher proton conductivity than BZY and increasing the content of Ce can improve the proton conductivity of BZCY [7], increasing the content of Ce could lead to a reduction of the stability of BZCY in an H_2O-containing atmosphere. Hence the long-term chemical stability of BZCY is still an issue, which restricts its practical application for H-SOECs. To date, in H-SOECs, researchers always use the same proton-conducting material for the

electrolyte and electrode (homogeneous design), which imposes limitations on the selection of materials and the improvement of the performance [4].

Furthermore, it should mention that BZY and BZCY possess not only proton conductivity but also non-negligible electronic conductivity, so the current leakage is an important concern of the application of H-SOECs. The current leakage in the electrolyte layer leads to a decrease of faradaic efficiency of electrolysis and energy efficiency of the total system[4]. To date, for H-SOECs, there are still paramount technical challenges of reducing the current leakage and improving the faradaic efficiency of electrolysis.

Here, according to the working principle of H-SOECs and the features of materials, a rational heterogeneous design is proposed for H-SOECs. In this heterogeneous design, the selection of materials is more flexible, compared with conventional homogeneous design. In this heterogeneous design, the excellent stability of BZY, as well as the high performance of BZCY, can be taken advantage of synchronously. Since the dense BZY electrolyte layer can protect the BZCY-Ni fuel electrode from steam in the air electrode side, the problem of instability of BZCY could be circumvented. Moreover, during sintering, the large shrinkage of BZCY-Ni is beneficial for the grain growth of BZY electrolyte, which could reduce the high resistance of the grain boundary of BZY. Furthermore, an interlayer could be formed in situ at the fuel electrode/electrolyte interface during high-temperature co-sintering. The rational control of the formation of this interlayer could offer some benefits, such as electron-blocking, improving the ionic conductivity of electrolyte layer, and more active interface [8]. As a result, this design concept could promote the cell electrochemical performance, the faradaic efficiency of electrolysis, and energy efficiency of the system.

In this study, to demonstrate the feasibility and advantages of this novel design, H-SOECs, with a configuration of $BaZr_{0.1}Ce_{0.7}Y_{0.2}O_3$(BZCY17)-Ni/BZY/$Sr_2Fe_{1.5}Mo_{0.5}O_{6-\delta}$(SFM)-BZY, have been assembled, as schematically shown in Fig.1. The fabrication of H-SOECs is studied in details. In addition, the electrochemical performance of H-SOECs is evaluated by recording the cell voltage-current relationship as well as the impedance spectra. The faradaic efficiency and energy efficiency of H-SOECs are calculated by developing a mathematical model.

2. Experimental

The experimental section mainly contains three parts, namely: synthesis and characterization of materials, fabrication of electrolysis cells, and characterization of electrolysis cells.

2. 1 Sythesis and characterization of materials

Glycine and citric acid assisted combustion method was used to synthesize the SFM powders [9]. Stoichiometric amounts of salt solution precursors $Sr(NO_3)_2$ (Alfa Aesar 99%), $Fe(NO_3)_3$ (Alfa Aesar 99%) and $(NH_4)_6Mo_7O_{24}\cdot 4H_2O$ (Alfa Aesar 99.9%) were mixed together in a beaker. Glycine (combustion-assisting chemicals) and citric acid (chelating agent) were added to the solution. The precursor solution was subsequently heated on a hot plate until self-combustion occurred. The as-prepared ash was fired at 1323 K for 5 h to form the perovskite structure.

The BZY and BZCY17 powders were synthesized by a combined EDTA-citric acid method [10]. Stoichiometric amounts of metal nitrate precursors $Ba(NO_3)_2$ (Alfa Aesar 99%), $ZrO(NO_3)_2\cdot xH_2O$ (Alfa Aesar 99.9%) and $Y(NO_3)_2\cdot 6H_2O$ (Alfa Aesar 99.9%) were dissolved in deionized water and titrated by ethylenediaminetetraacetic acid (EDTA). The precursor solution was subsequently heated on a hot plate until self-combustion occurred. The as-prepared ash was fired at 1373 K for 10 h to form the perovskite structure.

X-ray diffraction (Rigaku MiniFlex II, with Cu Kα radiation and a D/teX silicon strip detector) was used to evaluate the crystal structure of synthesized powders.

2. 2 Fabrication of electrolysis cells

NiO-based fuel electrode supported cells with thin BZY electrolyte and SFM-BZY air electrode were fabricated by dry-pressing, drop-coating and brush-painting method. NiO powders, BZY/BZCY17 powders and carbon black (average particle size: 1 μm) were mixed with a weight ratio of 5.5:4.5:2. The mixed powders were used to prepare the NiO-based fuel electrode substrates (10.4 mm in diameter and 0.3 mm in thickness after sintering at 1723 K) by dry-pressing and then firing at 873 K for 2 h. The shrinkage behavior of BZY-NiO and BZCY17-NiO substrates were analyzed using dilatometer measurement (Netzsch DIL 402 PC/4).

The BZY electrolyte slurry was prepared by ball milling BZY powders, using ethanol as solvent and adding other organic additives[11]. BZY electrolyte layer was then deposited on the NiO-based substrates by a drop-coating method and then sintering at 1723 K for 5 h. The SFM-BZY air electrode with an effective area of 0.33 cm^2 was applied onto the surface of the BZY electrolyte by brush-painting SFM-BZY paste and then sintering at 1373 K for 2 h.

2. 3 Characterization and test of electrolysis cells

Microstructures of the electrolysis cells were examined by scanning electron microscope (SEM, Zeiss Ultra Plus FESEM).

The experimental apparatus for the electrochemical test of electrolysis cells have be descripted in previous studies [12]. The prepared electrolysis cells were attached onto one end of an alumina tube using an electrical conductive paste (DAD-87, Shanghai Research Institute of Synthetic Resins, China) and high temperature ceramic adhesives (552-1105, Aremco, USA) as joining and sealing material, respectively. The gas mixture of H_2 and N_2 were fed to the fuel

electrode side, while air (3% H_2O) was introduced to the air electrode side. The flow rates of air, H_2 and N_2 were monitored by mass flow controllers (APEX, Schoonover, USA). Electrochemical characterizations for the electrolysis cells were conducted on an electrochemical test system (Versa STAT 3-400, Princeton Applied Research, USA). The *I-V* curves were recorded with a voltage sweep speed of 0.03 V s^{-1}.

3. Results and discussions

To demonstrate the feasibility and advantages of heterogeneous design, H-SOECs with homogeneous design have been fabricated for comparison. Electrolysis cells with these two kinds of designs are compared in terms of the properties of materials, electrochemical performance, and efficiency.

3. 1 Characterization of materials and electrolysis cells

The as-prepared BZY and BZCY17 powders are characterized by XRD, as shown in Fig.2. The XRD pattern of BZY shows a cubic perovskite structure, consistent with the literature[13], while the XRD pattern of BZCY17 reveals an orthorhombic perovskite structure, as described in the literature [14]. Besides, no secondary phases are observed in both samples, indicating that pure BZY and BZCY17 have been synthesized successfully.

Fig.3 shows the shrinkage curves of BZY-NiO and BZCY17-NiO fuel electrode. It is obvious that the temperature of obvious shrinkage is lower in the case of BZCY17-NiO, compared with BZY-NiO. After sintering at 1723 K, the shrinkage of BZCY17-NiO fuel electrode reaches 25% and the shrinkage of BZY-NiO fuel electrode is less than 18%, indicating that BZCY17-NiO possesses better sinterability than BZY-NiO. The inferior sinterability of BZY-NiO is due to the refractory nature of BZY, which has been reported [15]. Replacing BZY by BZCY17 is a feasible approach to improve the sinterability of the fuel electrode.

Fig.4 displays SEM images of the cross-section of electrolysis cells. Both cells are consisted of a porous NiO-based fuel electrode substrate and the thin BZY electrolyte layer. In these two kinds of cells, the thickness of electrolyte layers is similar, about 18μm, suggesting that the preparation of the electrolyte layer by the drop-coating method is reproducible. Comparing the BZY-NiO and BZCY17-NiO fuel electrode subtracts, it can be found that the size of pores in the BZY-NiO substrate is larger than that of BZCY17-NiO substrate. Since the pore former is the same in these two kinds of substrates, the larger size of pores in the BZY-NiO substrate is due to the smaller shrinkage of the substrate after sintering. The morphology of fuel electrode substrate mainly influences the gas transport in the fuel electrode and the concentration overpotential of H-SOECs. Since H_2, the molecule of which is very small, is the only product in the fuel electrode and the reduction of NiO greatly increases the porosity of fuel electrode, the effect of morphology of fuel electrode on the gas transport and overpotential of H-SOECs is insignificant. Therefore, the morphology difference between the BZY-Ni substrate and the BZCY17-Ni substrate has a negligible effect on the concentration overpotential of H-SOECs.

Moreover, it can be observed that there are more closed pores in the BZY electrolyte layer on the BZY-NiO substrate than that on the BZCY17-NiO substrate, indicating that the densification of BZY electrolyte layer on the former is worse than that on the latter. It is worth mentioning that oxygen molecules probably exist in these closed pores. It has been reported that the transport number of electron hole of BZY increase with the increasing partial pressure of oxygen, because high oxygen partial pressure is beneficial to the formation of electron hole, as shown in reaction (2) [16]. The concentration of electron hole is proportional to the $P_{O_2}^{\frac{1}{4}}$. Moreover, it is well known that the total conductivity of material is positively correlated to its densification. Therefore, the existence of closed pores may lead to the decrease of ionic transport number and total conductivity.

The surface morphology of the BZY electrolyte on different substrates is presented in Fig.5. In both cases, there are no obvious pores and the grains are tightly packed, suggesting that the electrolyte layers are dense enough to prevent the internal leakage of gas from one electrode side to the other electrode side. The most distinguished difference between these two electrolyte layers is the size of grains. The average size of grains of BZY electrolyte on the BZCY17-NiO substrate is about 0.8 μm, which is much larger than that on the BZY-NiO substrate (about 0.2 μm). It has been experimentally demonstrated that the size of grain has a significant effect on the conductivity of BZY and many other proton-conducting oxides because the resistance of grain bulk is substantially smaller than that of the grain boundary. Increasing the grain size of BZY is critical to achieving high proton conductivity [17].

To further investigate the influence of BZCY17-NiO substrate on the BZY electrolyte layer, the interaction between BZY and BZCY17 during high temperature sintering is studied by HRTEM. From Fig.6 (a) and (b), it can be seen that the lattice fringe spacings, corresponding to (110) plane of BZY and BZCY17, are 0.304 nm and 0.314 nm respectively. Then BZY and BZCY17 powders were mixed, followed by sintering at 1723 K. The mixture was also characterized by HRTEM, as shown in Fig.6 (c). The lattice spacing of the mixture, corresponding to (110) plane of the mixture, is 0.309 nm, which is between the values of BZY and BZCY17. This result confirms the interaction between BZY and BZCY17 and it is reasonable to deduce that Ce element could diffuse from the BZCY17-NiO substrate to the BZY electrolyte layer to form $BaZr_{0.8-x}Ce_xY_{0.2}O_3$ solid solution at the fuel electrode/electrolyte interface during sintering. It has been proved that increasing the content of Ce in $BaZr_{0.8-x}Ce_xY_{0.2}O_3$ can improve its sinterability and proton conductivity [18]. Hence $BaZr_{0.8-x}Ce_xY_{0.2}O_3$ interlayer possesses better sinterability and higher proton conductivity than the original BZY electrolyte. During high temperature sintering,

the shrinkage of interlayer and fuel electrode substrate can provide an extra driving force for the densification of the bulk BZY electrolyte layer, which is beneficial for the densification and grain growth of the electrolyte layer.

Consequently, combining the results of densification (Fig.4), size of grains (Fig.5) and the interaction (Fig.6), it is reasonable to expect that the conductivity of BZY electrolyte on the BZCY17-NiO substrate (heterogeneous design) is higher than that on the BZY-NiO substrate (homogeneous design).

3. 2 Electrochemical performance

The electrochemical performance of these two kinds of electrolysis cells is recorded and compared, as shown in Fig.7. From fig.7 (a), it can be seen that for both cells, the electrolysis current densities increase with the increase of the operation temperature and applied voltage. At the same temperature and voltage, the electrolysis current densities of cells with the heterogeneous design are always larger than those with the homogeneous design. Fig.7 (b) shows the electrolysis current density at 1.3 V and error analysis. The standard deviation of electrolysis current density at 1.3 V ranges from 6.0 mA cm^{-2} to 10.6 mA cm^{-2}. The range of standard deviation is reasonable, indicating that the test of electrochemical performance is accountable. For the cells with homogeneous design, the average electrolysis current densities at 1.3 V are 76 mA cm^{-2}, 186 mA cm^{-2} and 275 mA cm^{-2} at 823 K, 873 K and 923 K respectively. For the cells with heterogeneous design, the average electrolysis current densities at 1.3 V are 198 mA cm^{-2}, 377 mA cm^{-2} and 571 mA cm^{-2} at 823 K, 873 K and 923 K respectively, which are more than twice of those with homogeneous design.

Impedance spectra of electrolysis cells with different designs are measured under the OCV condition. Fig.8 (a) shows the impedance spectra at 923 K. Generally, when the electrolyte layer

is pure ion conductor, the intercept of the impedance spectra with the real axis at high-frequency corresponds to ohmic resistance of the electrolysis cell and the real axis range covered by the arc at lower frequency region represents the overall electrode polarization. However, when the electronic conductivity of electrolyte layer can't be negligible, the impedance spectra can't reflect the real ohmic resistance and polarization resistance without proper correction[19]. It has been theoretically[20] and experimentally[21] demonstrated that BZY possesses a high transport number of electron hole and non-negligible electronic conductivity in a dry atmosphere with high partial pressure of oxygen. Reaction (1) shows the formation of protonic defect ($OH_o^{\cdot}$) and reaction (2) presents the formation of electron hole ($h^{\cdot}$), as follows:

$$H_2O + V_O^{\cdot\cdot} + O_o = 2OH_o^{\cdot} \qquad (1)$$

$$\frac{1}{2}O_2 + V_O^{\cdot\cdot} = 2h^{\cdot} + O_o \qquad (2)$$

To evaluate the intrinsic resistances of electrolysis cells, a correction method has been developed [22]. Considering the electronic leakage in the electrolyte layer, an equivalent circuit for impedance spectra has been built, as shown in Fig.8 (b). The equivalent circuit contains R_i resistance which connects with one (RQ) element in series and with R_e resistance in parallel. The R_i and R_e stand for the ionic and electronic resistances in the electrolyte, respectively. The (RQ) element represents the electrode reactions and $R_{p,r}$ stands for the real polarization resistance. According to the equivalent circuit, the apparent ohmic resistance (R_s), obtained directly from impedance spectra, can be calculated as functions of R_i and R_e:

$$R_S = \frac{R_i R_e}{R_i + R_e} \qquad (I)$$

The total apparent resistance (R_T), obtained directly from impedance spectra, can be derived by using the following equation:

$$R_T = \frac{(R_i + R_{p,r})R_e}{(R_i + R_{p,r}) + R_e} \qquad (II)$$

The transport number of ions (t_i) can be determined by using the equation below:

$$t_i = \frac{R_e}{R_i+R_e} = \frac{V_{ocv}}{E_N}(1 + \frac{R_{p,r}}{R_i+R_e}) \qquad \text{(III)}$$

where V_{ocv} is the open circuit voltage and E_N is the theoretical Nernst potential.

$R_{p,r}$ can be solved from equation II and III:

$$R_{p,r} = \frac{(R_T-R_S)R_S}{t_i[t_iR_T-(R_T-R_S)]} \qquad \text{(IV)}$$

From equation IV, it can be easily derived that only when t_i=1, $R_{p,r}$ is equal to (R_T-R_s), meaning that $R_{p,r}$ and apparent polarization resistance (R_p) are identical. When t_i<1 (not pure ion conductor), $\frac{R_{p,r}}{R_p} = \frac{R_S}{t_i[t_iR_T-(R_T-R_S)]} > 1$, indicating that the $R_{p,r}$ is larger than the R_p.

$R_{p,r}$, R_i and R_e can be solved from equation I, II and III, as following:

$$R_{p,r} = \frac{R_T-R_S}{\frac{V_{ocv}}{E_N}[1-\frac{R_S}{R_T}(1-\frac{V_{ocv}}{E_N})]} \qquad \text{(V)}$$

$$R_i = \frac{R_SR_e}{R_e-R_S} = \frac{R_S}{1-\frac{R_S}{R_T}(1-\frac{V_{ocv}}{E_N})} \qquad \text{(VI)}$$

$$R_e = \frac{R_T}{1-\frac{V_{ocv}}{E_N}} \qquad \text{(VII)}$$

The calculation results for cells with homogeneous design and heterogeneous design are shown in table 1 and table 2, respectively. For both cells, it can be seen that the $R_{p,r}$ is larger than the R_p and R_i is larger than the R_s, which is consistent with the theoretical expectation. The main difference between these two kinds of electrolysis cells is the R_i. The R_i of electrolysis cells with the heterogeneous design are always smaller than those with the homogeneous design. For example, the R_i of cells with heterogeneous design is 0.846 Ω cm^2 at 873 K, which is much smaller than that with homogeneous design (2.038 Ω cm^2). In other words, the ionic conductivity of the electrolyte layer on the BZCY17-NiO substrates reaches to 2.13×10^{-3} S cm^{-1} at 873 K, which is significantly larger than that on the BZY-Ni substrates (0.88×10^{-3} S cm^{-1}). These results

demonstrate that the application of heterogeneous design is beneficial for improving the ionic conductivity of the BZY electrolyte layer, which is due to the better sinterability of BZCY17-NiO substrate and the formation of $BaZr_{0.8-x}Ce_xY_{0.2}O_3$ interlayer. The comparison of conductivity of BZY electrolyte, fabricated by different approaches, is shown in table 3. The conductivity of BZY electrolyte of heterogeneous design is higher than that fabricated by pulsed laser deposition (PLD) [23]and comparable with those fabricated by using sintering aid of ZnO[24] and CaO[25] or ionic diffusion strategy [26]. It has been reported that adding sintering aid leads to a decrease of the ionic transport number of BZY electrolyte[27], which is detrimental to the efficiency of electrolysis. Moreover, for ionic diffusion strategy, extra metal oxide (In_2O_3) is needed, which could increase the cost of fabrication. Therefore, applying heterogeneous design is a cost-effective and simple method to fabricate dense BZY electrolyte with high proton conductivity.

Besides R_i, the real polarization resistances ($R_{p,r}$) of electrolysis cells become smaller, when heterogeneous design is applied, compared with homogeneous design. For example, the $R_{p,r}$ in the case of heterogeneous design (3.012 Ω cm^2) is slightly smaller than that of homogeneous design (3.480 Ω cm^2) at 873 K. It has been demonstrated that the ionic conductivity of electrolyte not only determines the resistance of electrolyte, but also affects the polarization resistance of electrode. Increasing the ionic conductivity of electrolyte could accelerate the transfer of ions between the electrolyte/electrode interface or improve kinetics of the electrode reaction taking place at the boundaries between electrolyte and electrode [28]. Therefore, the smaller polarization resistances in the case of heterogeneous design are attributed to the electrolyte layer with higher ionic conductivity.

From table 1 and 2, it can be also seen that the ionic transport number (t_i) of electrolyte on both cases decreases with increasing the temperatures, implying that the electronic conductivity of

electrolyte becomes more significant with temperatures. Furthermore, the transport number of ions (t_i) of the electrolyte on BZCY17-Ni substrates is slightly larger than those on BZY-Ni substrates. Larger t_i means the ionic conductivity of electrolyte is more predominant and electronic conductivity of electrolyte is less significant, which is beneficial for reducing the electronic leakage in the electrolyte layer and improving the energy efficiency of H-SOECs. The larger t_i in the cases with heterogeneous design is probably due to less closed pores and the diffusion of small amount of Ce from the BZCY17-Ni substrate to the electrolyte layer. Similar experimental results have also been observed. The electronic leakage in $BaZr_{0.8}Ce_{0.1}Y_{0.1}O_3$ membrane is slightly smaller than that in the $BaZr_{0.9}Y_{0.1}O_3$ membrane [29].

The stability of H-SOECs with heterogeneous design is studied at 1.3 V and 873 K, as shown in Fig. 9. At the beginning of the stability test, the absolute current density increases from 380 mA cm^{-2} to 408 mA cm^{-2}. Then it becomes stable at about -370 mA cm^{-2} in the rest of the test, demonstrating that electrolysis cells show stable performance. The change of performance at the beginning may be due to the activation of electrode, the change of sealing condition of electrolysis cells and the evaporation of silver current collector.

3. 3 Faradiac and energy efficiency

To roughly evaluate the energy efficiency of H-SOECs, an electrochemical model of H-SOECs is built. Since the conductivity of electron hole in the BZY electrolyte can't be neglected, not only proton conductivity ($\sigma_{OH^{\cdot}}$) but also electronic conductivity ($\sigma_{h^{\cdot}}$) of BZY electrolyte must be considered in the electrochemical model. It has been experimentally demonstrated that the electronic conductivity ($\sigma_{h^{\cdot}}$) of perovskite proton conductor changes with external voltage [30]. And it has been theoretically deduced that the conductivity of electron hole is a function of cell potential (E), as shown in equation (VIII) [31]:

$$\sigma_{h\cdot} = \sigma_{h\cdot}^{o} \exp\left(\frac{F(E-V_{ocv})}{RT}\right) \qquad \text{(VIII)}$$

where R is the ideal gas constant, T is temperature, F is the faraday constant, $\sigma_{h\cdot}^{o}$ is the conductivity of electron hole under OCV.

The current densities of proton ($J_{OH\cdot}$) and electron hole ($J_{h\cdot}$) occuring in the electrolyte can be expressed by the Nernst-Planck equation, as shown in equation (IX) and (X) [32]:

$$J_{OH\cdot} = -\frac{\sigma_{OH\cdot}}{F}\frac{\partial \mu_{OH\cdot}}{\partial x} - \sigma_{OH\cdot}\frac{\partial \phi(x)}{\partial x} \qquad \text{(IX)}$$

$$J_{h\cdot} = -\frac{\sigma_{h\cdot}}{F}\frac{\partial \mu_{h\cdot}}{\partial x} - \sigma_{h\cdot}\frac{\partial \phi(x)}{\partial x} \qquad \text{(X)}$$

where μ_X is the chemical potential of X, ϕ is the electrostatic potential. Combining equation (VIII), (IX) and (X), and then integrating, the numercial solution of $J_{OH\cdot}$ and $J_{h\cdot}$can be obtained. Defining the direction of $J_{h\cdot}$ is positive, the external current density can be determined according to Kirchhoff's law, as shown in equation (XI):

$$J_{ext} = -(J_{h\cdot} + J_{OH\cdot}) \qquad \text{(XI)}$$

Thus the faradaic efficiency (FE) of electrolysis can be calculated by the following equations:

$$FE = \frac{N_{H_2}}{|J_{ext}| \times t/nF} = \frac{J_{OH_o}}{|J_{ext}|} \qquad \text{(XII)}$$

where J_{ext} is the external current density, N_{H_2} is the production rate of hydrogen, n is the number of electron envolved in the reaction and t is time. The energy efficiency of H-SOECs, which is defined as the ratio of energy output and energy input, is calculated by the following equation:

$$\eta = \frac{N_{H_2} \times LHV_{H_2}}{E_{ele} + E_{heat}} \qquad \text{(XIII)}$$

where LHV_{H_2} is the lower heating value of hydrogen, E_{ele} is the electricity input and E_{heat} is the heat required for the process.

The faradaic efficiency and energy efficiency of H-SOECs are calculated, as shown in Fig. 10 (a) and (b). The faradaic efficiencies of H-SOECs with homogeneous design and heterogeneous

design are compared in Fig.10 (a). For both electrolysis cells, the faradaic efficiency decreases with increasing operating temperature, which is due to the decreasing of ionic transport number(t_i) with temperature, as shown in table 1 and 2. Moreover, it is obvious that the faradaic efficiency in the case of heterogeneous design is always higher than that in the case of homogeneous design. For example, at 1.3 V and 823 K, the faradaic efficiency of heterogeneous design (54.0%) is higher than that of homogeneous design (44.0%). The higher faradaic efficiency of heterogeneous design is attributed to the larger t_i of the electrolyte on BZCY17-Ni substrates, compared with that on BZY-Ni. Larger t_i means the ionic current in the electrolyte is more predominant and the electronic current is less significant.

The calculated results of energy efficiency are presented in Fig. 10(b). The energy efficiency is highly related to the faradaic efficiency and it shows a similar trend with the faradaic efficiency. For both electrolysis cells, the energy efficiency decreases with operating temperature. This can be explained by the fact that although the electricity input can be saved at a higher temperature due to less resistance of electrolysis cells, the faradaic efficiency decreases with the increase of temperate, resulting in a decrease of efficiency of electricity input. Moreover, it can be found that higher energy efficiency is achieved in the case of heterogeneous design. For example, at 823 K and 1.3 V, the energy efficiency of heterogeneous design is 48.5%, which is higher than that of homogeneous design (40.6%). The better performance of electrolysis (less electricity input) and larger ionic transport number (t_i) of the electrolyte both contribute to the higher energy efficiency of electrolysis cells with heterogeneous design.

4. Conclusion

In this work, the feasibility and advantages of the heterogeneous design for H-SOECs have been investigated and demonstrated in electrolysis cells with $BaZr_{0.1}Ce_{0.7}Y_{0.2}O_3$(BZCY17)-Ni as

the fuel electrode material and $BaZr_{0.8}Y_{0.2}O_{3-\delta}$ (BZY) as the electrolyte material by experiment and modeling. In this heterogeneous design, the merits of BZY and BZCY17 can be taken advantage of, and the drawbacks of them can be circumvented simultaneously. The experimental results show that during high temperature sintering，the BZCY17-NiO substrate can provide a large driving force for the densification of the BZY electrolyte layer, resulting in grain growth of BZY and smaller resistance of grain boundary. In addition, the HRTEM analysis demonstrates the in-situ formation of $BaZr_{0.8-x}Ce_xY_{0.2}O_3$ solid solution at the fuel electrode/electrolyte interface, which is beneficial for improving the electrochemical performance. At 873 K, the BZY electrolyte layer of the heterogeneous design shows high ionic conductivity of 2.13×10^{-3} S cm^{-1}, which is more than twice of that of homogeneous design (0.88×10^{-3} S cm^{-1}). The H-SOECs with heterogeneous design exhibit better electrolysis performance than those with homogeneous design. Moreover, the ionic transport number of BZY electrolyte layer is increased slightly by applying the heterogeneous design. As a result, higher faradaic efficiency and energy efficiency are achieved in the H-SOECs with the heterogeneous design. This work demonstrates a rational design for high-performance H-SOECs.

Acknowledgements

This work was primarily supported by the US National Science Foundation (DMR–1832809), National Natural Science Foundation of China (Grant Nos.: 21406190 and 21878257) and Natural Science Foundation of the Higher Education Institutions of Jiangsu Province (No. 18KJA430017).

References

[1] Y. Wang, T. Liu, L. Lei, F. Chen. High temperature solid oxide H_2O/CO_2 co-electrolysis for syngas production. Fuel Processing Technology. 161 (2017) 248-58.

[2] Y. Luo, Y. Shi, W. Li, N. Cai. Synchronous enhancement of H_2O/CO_2 co-electrolysis and methanation for efficient one-step power-to-methane. Energy Conversion and Management. 165 (2018) 127-36.

[3] N. Danilov, J. Lyagaeva, G. Vdovin, E. Pikalova, D. Medvedev. Electricity/hydrogen conversion by the means of a protonic ceramic electrolysis cell with $Nd_2NiO_{4+\delta}$ -based oxygen electrode. Energy Conversion and Management. 172 (2018) 129-37.

[4] L. Lei, J. Zhang, Z. Yuan, J. Liu, M. Ni, F. Chen. Progress Report on Proton Conducting Solid Oxide Electrolysis Cells. Advanced Functional Materials. (2019) 1903805.

[5] L. Bi, S.P. Shafi, E. Traversa. Y-doped $BaZrO_3$ as a chemically stable electrolyte for proton-conducting solid oxide electrolysis cells (SOECs). Journal of Materials Chemistry A. 3 (2015) 5815-9.

[6] H. Dai, H. Kou, H. Wang, L. Bi. Electrochemical performance of protonic ceramic fuel cells with stable BaZrO3-based electrolyte: A mini-review. Electrochemistry Communications. 96 (2018) 11-5.

[7] Y. Guo, Y. Lin, R. Ran, Z. Shao. Zirconium doping effect on the performance of proton-conducting $BaZryCe_{0.8-y}Y_{0.2}O_{3-\delta}$ ($0.0 \leq y \leq 0.8$) for fuel cell applications. Journal of Power Sources. 193 (2009) 400-7.

[8] W. Sun, Z. Shi, J. Qian, Z. Wang, W. Liu. In-situ formed $Ce_{0.8}Sm_{0.2}O_{2-\delta}$@Ba(Ce, Zr)$_{1-x}(Sm,Y)_xO_{3-\delta}$ core/shell electron-blocking layer towards $Ce_{0.8}Sm_{0.2}O_{2-\delta}$-based solid oxide fuel cells with high open circuit voltages. Nano Energy. 8 (2014) 305-11.

[9] T. Liu, Y. Zhao, X. Zhang, H. Zhang, G. Jiang, W. Zhao, et al. Robust redox-reversible perovskite type steam electrolyser electrode decorated with in situ exsolved metallic nanoparticles. Journal of Materials Chemistry A. (2019).

[10] L. Lei, Z. Tao, X. Wang, J.P. Lemmon, F. Chen. Intermediate-temperature solid oxide electrolysis cells with thin proton-conducting electrolyte and a robust air electrode. Journal of Materials Chemistry A. 5 (2017) 22945-51.

[11] L. Lei, Z. Tao, T. Hong, X. Wang, F. Chen. A highly active hybrid catalyst modified $(La_{0.60}Sr_{0.40})_{0.95}Co_{0.20}Fe_{0.80}O_{3-\delta}$ cathode for proton conducting solid oxide fuel cells. Journal of Power Sources. 389 (2018) 1-7.

[12] L. Lei, Y. Wang, S. Fang, C. Ren, T. Liu, F. Chen. Efficient syngas generation for electricity storage through carbon gasification assisted solid oxide co-electrolysis. Applied Energy. 173 (2016) 52-8.

[13] L. Lei, J.M. Keels, Z. Tao, J. Zhang, F. Chen. Thermodynamic and experimental assessment of proton conducting solid oxide fuel cells with internal methane steam reforming. Applied Energy. 224 (2018) 280-8.

[14] Z. Tao, B. Wang, G. Hou, N. Xu. Preparation of $BaZr_{0.1}Ce_{0.7}Y_{0.2}O_{3-\delta}$ thin membrane based on a novel method-drop coating. International Journal of Hydrogen Energy. 39 (2014) 16020-4.

[15] L. Bi, E.H. Da'as, S.P. Shafi. Proton-conducting solid oxide fuel cell (SOFC) with Y-doped $BaZrO_3$ electrolyte. Electrochemistry Communications. 80 (2017) 20-3.

[16] D. Han, Y. Noda, T. Onishi, N. Hatada, M. Majima, T. Uda. Transport properties of acceptor-doped barium zirconate by electromotive force measurements. International Journal of Hydrogen Energy. 41 (2016) 14897-908.

[17] J. Tong, D. Clark, L. Bernau, M. Sanders, R. O'Hayre. Solid-state reactive sintering mechanism for large-grained yttrium-doped barium zirconate proton conducting ceramics. Journal of Materials Chemistry. 20 (2010) 6333-41.

[18] N. Kochetova, I. Animitsa, D. Medvedev, A. Demin, P. Tsiakaras. Recent activity in the development of proton-conducting oxides for high-temperature applications. RSC Advances. 6 (2016) 73222-68.

[19] D. Poetzsch, R. Merkle, J. Maier. Investigation of oxygen exchange kinetics in proton-conducting ceramic fuel cells: Effect of electronic leakage current using symmetric cells. Journal of Power Sources. 242 (2013) 784-9.

[20] H. Zhu, S. Ricote, C. Duan, R.P. O'Hayre, D.S. Tsvetkov, R.J. Kee. Defect Incorporation and Transport within Dense $BaZr_{0.8}Y_{0.2}O_{3-\delta}$ (BZY20) Proton-Conducting Membranes. Journal of The Electrochemical Society. 165 (2018) F581-F8.

[21] D. Han, T. Uda. The best composition of an Y-doped $BaZrO_3$ electrolyte: selection criteria from transport properties, microstructure, and phase behavior. Journal of Materials Chemistry A. 6 (2018) 18571-82.

[22] J. Zhang, L. Lei, F. Zhao, F. Chen, M. Han. A novel equivalent circuit for GDC-based solid oxide cells considering the variations of cell resistances under load. Electrochimica Acta. 340 (2020).

[23] D. Pergolesi, E. Fabbri, E. Traversa. Chemically stable anode-supported solid oxide fuel cells based on Y-doped barium zirconate thin films having improved performance. Electrochemistry Communications. 12 (2010) 977-80.

[24] I. Luisetto, S. Licoccia, A. D'Epifanio, A. Sanson, E. Mercadelli, E. Di Bartolomeo. Electrochemical performance of spin coated dense $BaZr_{0.80}Y_{0.16}Zn_{0.04}O_{3-\delta}$ membranes. Journal of Power Sources. 220 (2012) 280-5.

[25] Z. Sun, E. Fabbri, L. Bi, E. Traversa, R. Koc. Electrochemical Properties and Intermediate-Temperature Fuel Cell Performance of Dense Yttrium-Doped Barium Zirconate with Calcium Addition. Journal of the American Ceramic Society. 95 (2012) 627-35.

[26] L. Bi, E. Fabbri, Z. Sun, E. Traversa. A novel ionic diffusion strategy to fabricate high-performance anode-supported solid oxidefuel cells (SOFCs) with proton-conducting Y-doped $BaZrO_3$ films. Energy & Environmental Science. 4 (2011) 409-12.

[27] D. Han, S. Uemura, C. Hiraiwa, M. Majima, T. Uda. Detrimental Effect of Sintering Additives on Conducting Ceramics: Yttrium-Doped Barium Zirconate. ChemSusChem. 11 (2018) 4102-13.

[28] W. Li, M. Gong, X. Liu. Characterization of Doped Yttrium Chromites as Electrodes for Solid Oxide Fuel Cell by Impedance Method. Journal of The Electrochemical Society. 161 (2014) F551-F60.

[29] M. Dippon, S.M. Babiniec, H. Ding, S. Ricote, N.P. Sullivan. Exploring electronic conduction through $BaCe_xZr_{0.9-x}Y_{0.1}O_{3-d}$ proton-conducting ceramics. Solid State Ionics. 286 (2016) 117-21.

[30] D. Huan, W. Wang, Y. Xie, N. Shi, Y. Wan, C. Xia, et al. Investigation of real polarization resistance for electrode performance in proton-conducting electrolysis cells. Journal of Materials Chemistry A. 6 (2018) 18508-17.

[31] E. Vøllestad, R. Strandbakke, M. Tarach, D. Catalán-Martínez, M.-L. Fontaine, D. Beeaff, et al. Mixed proton and electron conducting double perovskite anodes for stable and efficient tubular proton ceramic electrolysers. Nature materials. (2019) 1.

[32] J.-H. Zhang, L.-B. Lei, D. Liu, F.-Y. Zhao, M. Ni, F. Chen. Mathematical modeling of a proton-conducting solid oxide fuel cell with current leakage. Journal of Power Sources. 400 (2018) 333-40.

Captions:

Fig.1 Schematic of H-SOECs with homogeneous and heterogeneous design.

Fig.2 XRD patterns of BZY and BZCY17.

Fig.3 Shrinkage behavior of BZY-NiO and BZCY17-NiO fuel electrode.

Fig.4 Cross section images of electrolysis cells (a) with BZY-NiO fuel electrode (homogeneous design); (b) with BZCY17-NiO fuel electrode (heterogeneous design).

Fig.5 Surface morphology of BZY electrolyte (a) on the BZY-NiO substrate (homogeneous design); (b) on the BZCY17-NiO substrate (heterogeneous design).

Fig.6 HRTEM images (a) BZY; (b) BZCY17; (c) mixture of BZY and BZCY17.

Fig.7 (a) I-V curves of H-SOECs (3%H_2O-air in the air electrode, 80%N_2-20%H_2 in the fuel electrode); (b) electrolysis current at 1.3 V and error analysis

Fig.8 Impedance spectra (a) with homogeneous and heterogeneous design at 923 K; (b) an equivalent circuit.

Fig.9 Short term stability test of H-SOECs with heterogeneous design at 873 K.

Fig.10 (a) Analysis of Faradaic efficiency; (b) analysis of Energy efficiency.

Table 1 Analysis of impedance spectra of electrolysis cells with homogeneous design

Table 2 Analysis of impedance spectra of electrolysis cells with heterogeneous design

Table 3 Comparison of conductivity of BZY electrolyte layer at 873 K

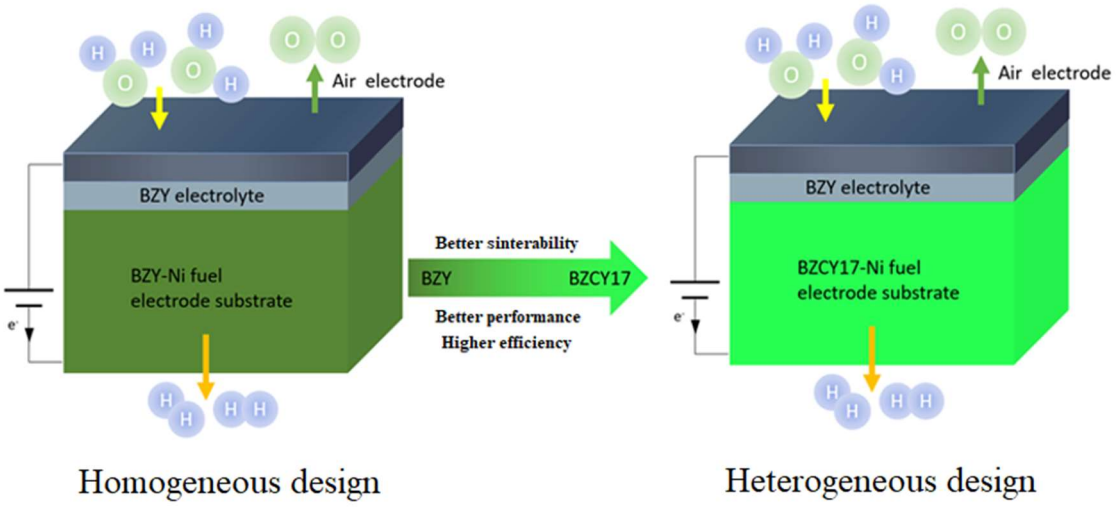

Fig.1 Schematic of H-SOECs with homogeneous and heterogeneous design.

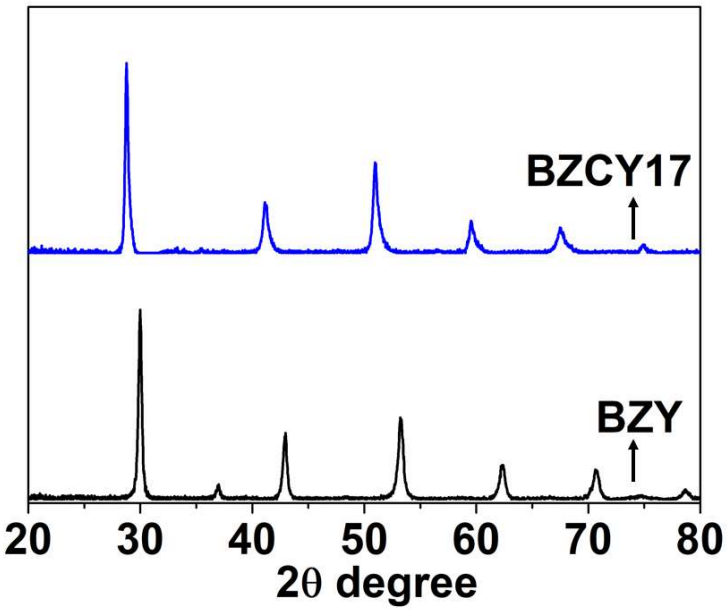

Fig.2 XRD patterns of BZY and BZCY17.

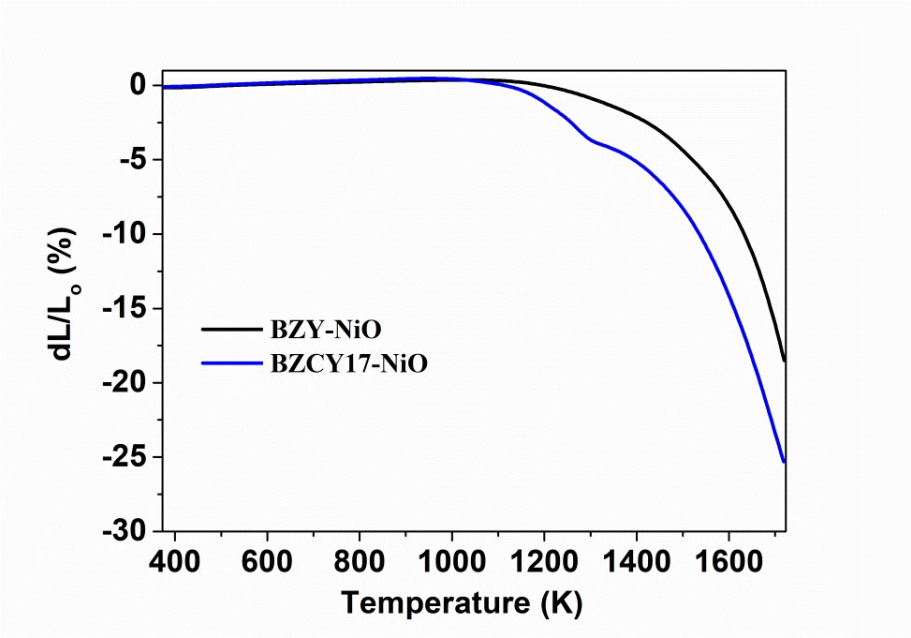

Fig.3 Shrinkage behavior of BZY-NiO and BZCY17-NiO fuel electrode.

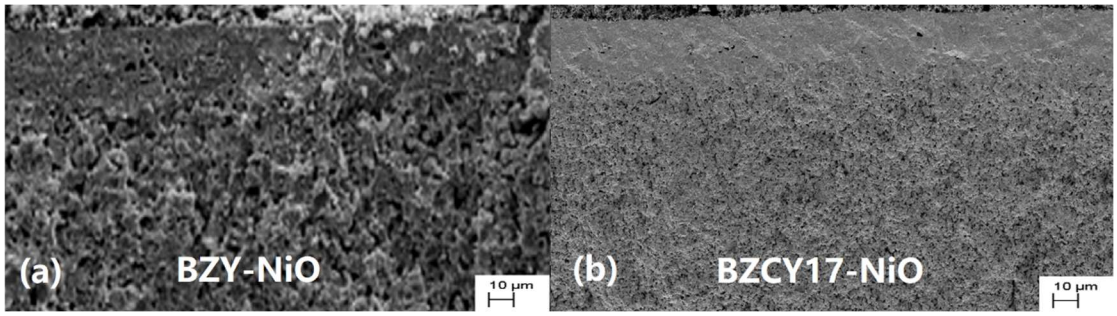

Fig.4 Cross section images of electrolysis cells (a) with BZY-NiO fuel electrode (homogeneous design); (b) with BZCY17-NiO fuel electrode (heterogeneous design).

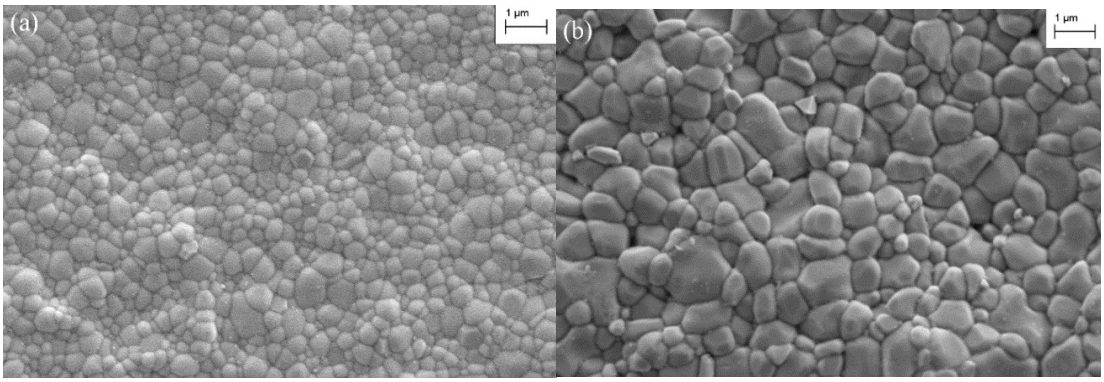

Fig.5 Surface morphology of BZY electrolyte (a) on the BZY-NiO substrate (homogeneous design); (b) on the BZCY17-NiO substrate (heterogeneous design).

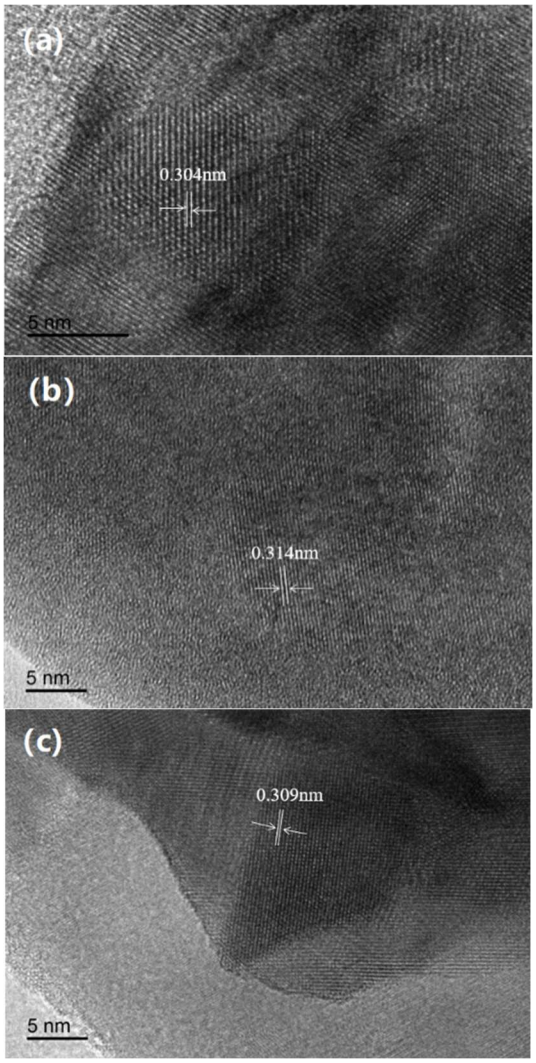

Fig.6 HRTEM images (a) BZY; (b) BZCY17; (c) mixture of BZY and BZCY17.

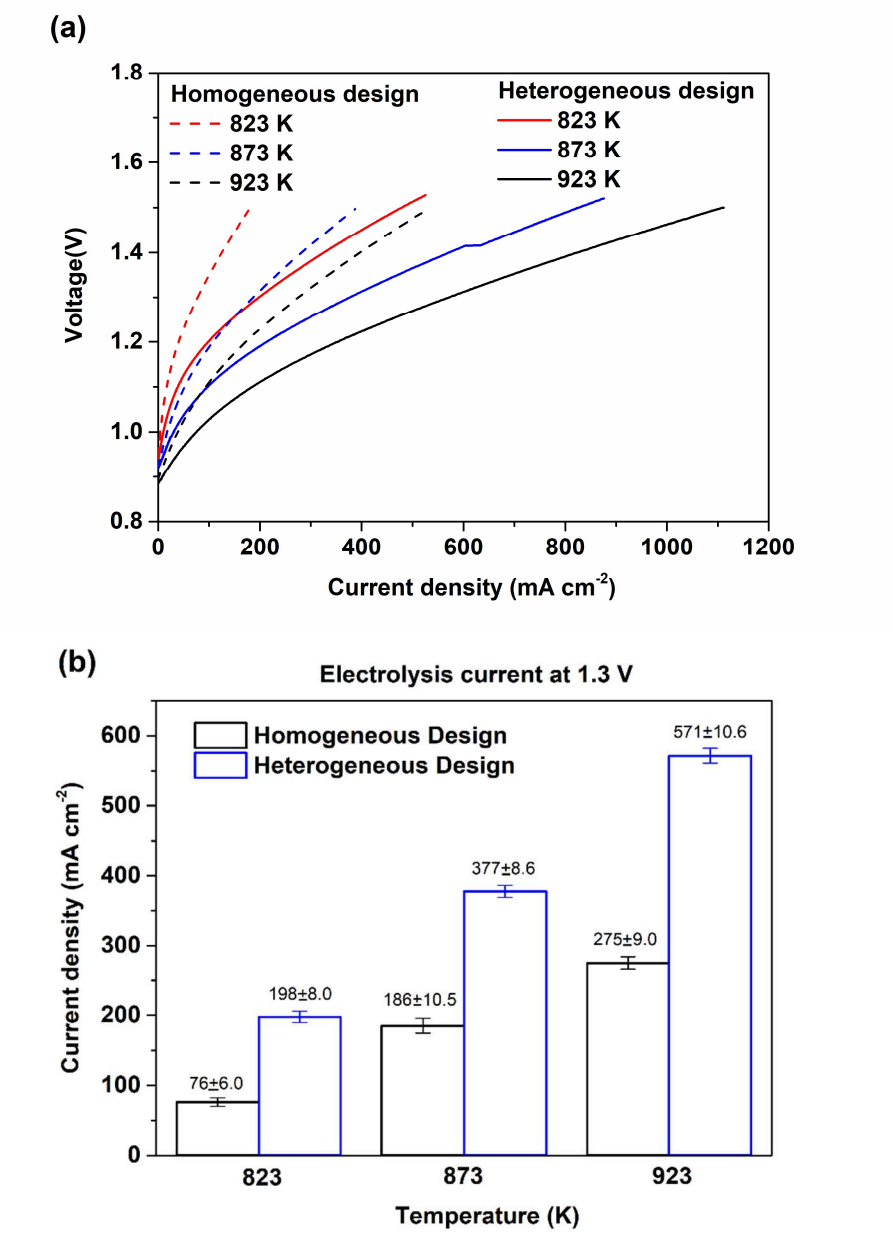

Fig.7 (a) I-V curves of H-SOECs (3%H_2O-air in the air electrode, 80%N_2-20%H_2 in the fuel electrode); (b) electrolysis current at 1.3 V and error analysis

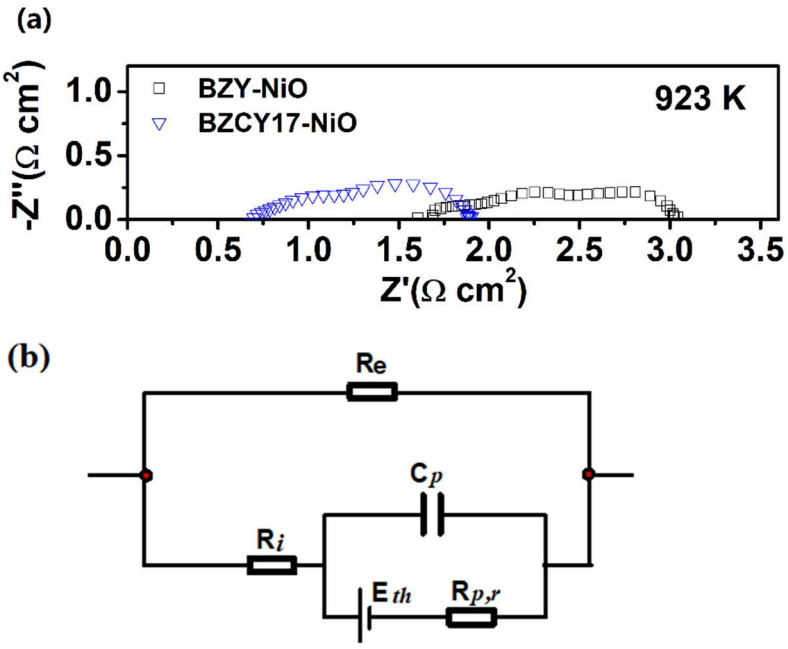

Fig.8 Impedance spectra (a) with homogeneous and heterogeneous design at 923 K; (b) an equivalent circuit.

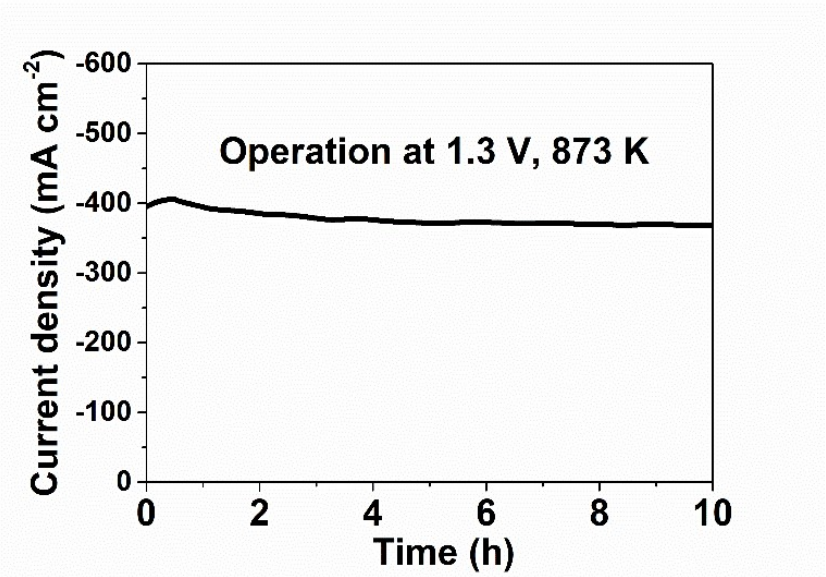

Fig.9 Short term stability test of H-SOECs with heterogeneous design at 873 K.

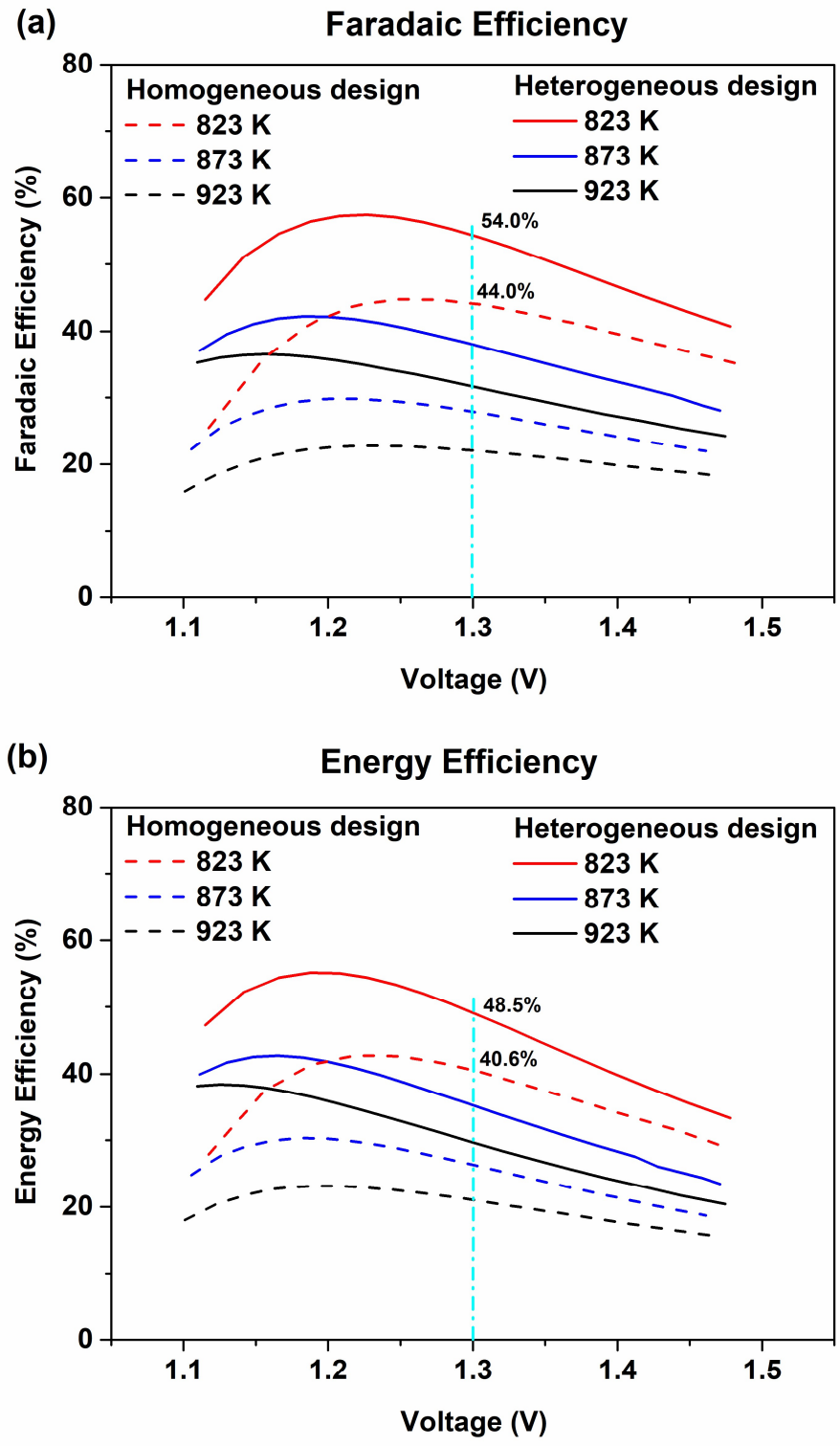

Fig.10 (a) Analysis of Faradaic efficiency; (b) analysis of Energy efficiency.

Table 1 Analysis of impedance spectra of electrolysis cells with homogeneous design

Temperature (K)	E_N (V)	V_{OCV} (V)	R_p (Ω cm^2)	R_s (Ω cm^2)	$R_{p,r}$ (Ω cm^2)	R_e (Ω cm^2)	R_i (Ω cm^2)	t_i
823	1.086	0.948	6.660	2.350	7.892	70.832	2.431	0.967
873	1.075	0.921	2.810	1.920	3.480	33.104	2.038	0.942
923	1.063	0.894	1.440	1.600	1.868	19.140	1.746	0.916

Table 2 Analysis of impedance spectra of electrolysis cells with heterogeneous design

Temperature (K)	E_N (V)	V_{OCV} (V)	R_p (Ω cm^2)	R_s (Ω cm^2)	$R_{p,r}$ (Ω cm^2)	R_e (Ω cm^2)	R_i (Ω cm^2)	t_i
823	1.086	0.941	5.838	0.972	6.870	50.955	0.991	0.981
873	1.075	0.919	2.484	0.816	3.012	22.799	0.846	0.964
923	1.063	0.880	1.200	0.699	1.547	11.041	0.746	0.937

Table 3 Comparison of conductivity of BZY electrolyte layer at 873 K

Configuration of cells	Fabrication process	Conductivity (S cm^{-1})	[Ref]
Ni-BZY/BZY (4 μm)	Pulsed laser deposition (PLD)	0.22×10^{-3}	[23]
Ni-BZY/BZY (20 μm)	Ionic diffusion strategy	2.27×10^{-3}	[26]
Ni-BZY/BZY_ZnO (20 μm)	ZnO as sintering aid	2.0×10^{-3}	[24]
Ni-BZY/BZY_CaO (25 μm)	CaO as sintering aid	1.67×10^{-3}	[25]
Homogeneous design (18 μm)	Simple co-sintering	0.88×10^{-3}	This study
Heterogeneous design (18 μm)	Simple co-sintering	2.13×10^{-3}	This study